Journal of Rajasthan Academy of Physical Sciences
ISSN: 0972-6306; URL: http://raops.org.in
Vol.24, No.1&2, January-June, 2025, 43-57

PRECISE REFINEMENT OF CRYSTAL STRUCTURE AND SIZE-STRAIN PARAMETERS OF ULTRAFINE ZRO_2 NANOPARTICLES

Vinod Kumar[1], Manisha[2] and **S. Kumar[3]**
[1,2,3]Department of Physics, Mohanlal Sukhadia University, Udaipur-31300, India.
Email: skphy@mlsu.ac.in[3]

Abstract: Detailed nano-structural characterization of nanomaterials is an important issue since it enables precise understanding of the chemical, optical, electronic, magnetic and other physical properties for their possible utilization/integration into modern multifunctional devices and technology. Accurate determination of the crystallographical parameters, crystallite shape & size, micro strain, dislocation density of nanoparticles is the first step of characterization of nanomaterials. In this article, we have refined the X-ray diffraction (XRD) data of ultrafine ZrO_2 nanoparticles (NPs) using least square technique based PowderX and Rietveld profile analysis for the precise extraction of the crystallographic parameters. PowderX analysis suggested both cubic and tetragonal crystal structure of ZrO_2 NPs due to too much similarity in the two phases. Notably, best fitted Rietveld refinement affirmed tetragonal structure (Space group P 42/nmc (No. 137), Z=2) of ultrafine ZrO_2 NPs. Size and strain parameters of ultrafine ZrO_2 NPs were precisely estimated using eight different models and well compared with the HRTEM micrograph analysis. The analysis yielded 6 (±2) nm size and lattice strain of 3.14×10^{-3} the ultrafine ZrO_2 NPs. It is concluded that Rietveld, WHF analysis and lognormal size distribution of ultrafine NPs are most appropriate techniques for estimating the crystal structure and size-strain parameters ZrO_2 NPs.

Key Words: ZrO_2 NPs; PowderX, Rietveld, Tetragonal, lattice strain

1. Introduction

The zirconia (ZrO_2) based systems are being continuously explored for decades both for the fundamental understanding as well as for applied research. ZrO_2 is generally recognized as the prototype steel ceramic in the broad family of the ceramics with good thermal & chemical stability and great mechanical strength [2,3,4,5,14,15]. Aside the fundamental importance of ZrO_2 in understanding the mechanical, chemical and thermal properties, it has other important practical technological applications in the diverse fields such as gas sensors, solar cells, photovoltaic, photo-catalysts, resistors, semiconductor devices, electrode material for supercapacitors, magnetic storage and dental implantation & teeth engineering along with other biomedical engineering like antimicrobial agent etc.

Studies on ZrO_2 have shown strong dependence of its behaviour on the quantum size effect, morphology and crystallography of the ZrO_2. Detailed structural analysis along with size-strain characterization of nanomaterials is an important issue since it enables precise understanding of the chemical, optical, electronic, magnetic and other physical properties for their possible utilization/integration into modern multifunctional devices and technology. Accurate determination of the crystallographical parameters, crystallite shape & size, micro strain, dislocation density of nanoparticles is first step of the characterization of newly synthesized nanomaterials. Over the years, number of theoretical & experimental studies has been made for tuning the chemical, physical and biomedical properties of ZrO_2. The purpose of this paper is to comprehensively analyse its nano-structural properties using various strategies. In this article, we have accurately determined the tetragonal crystal structure and size-strain parameters of ultrafine ZrO_2 NPs derived by simple green solution-combustion reactions. Findings are extensively discussed and hope our study will motivate future experimental investigations on ZrO_2 based nanomaterials.

2. Experimental details

A nanocrystalline sample of ZrO_2 NPs was synthesized using green chemistry based self-combustion route and characterized using powder X-ray diffractometry (XRD) and high-resolution transmission electron microscopy (HRTEM) measurements at room temperature [1,7,8,11,16,17]. The data were analysed using PowderX, FullProf suite of programs and origin software [9,10].

In the powder analysis, initially the positions of Bragg peaks were marked and then position of Bragg peaks were calculated using the available of information with JCPDS card. In the second step the observed and calculated d-spacings of the Bragg peaks are matched and according miller indices assigned to the observed Bragg peaks. In the last cycle, the cell parameters from each Bragg planes are calculated and then lattice parameter were refined using least square fit [6].

In the Rietveld refinement, initially crystallographical information corresponding to most appropriate space group (as per powder-X analysis & JCPDS card) is taken as initial guess parameters. In the first step of refinement, scale factor, 2θ zero correction, background and instrumental parameters were varied and in the second round the structural parameters were included and refined. Finally, all the parameters were varied upon achieving the convergence in less than ten cycles [10].

3. Result and discussion

3.1 Structural: XRD analysis

Fig. 1 illustrates sharp and well resolved Bragg reflections in the XRD pattern of ZrO_2 NPs. This XRD pattern indicates for good crystallinity of the ZrO_2 NPs. In the first step of data analysis, the positions of Bragg peaks (marked in Fig.1) were computed and compared with the JCPDS CAS No. 27-0997, 17-0923 and 37-1484 corresponding to Cubic, Tetragonal and Monoclinic phases of zirconia, respectively. Positions of all

observed reflections were matched well with the cubic and tetragonal phase but did not match with monoclinic phase. So, the XRD data were treated with the Powder X program. Accordingly, all the observed peaks were nicely indexed in the cubic as well as tetragonal symmetry. Further, the obtained fcc lattice parameters (a = 5.117 (2) Å and V = 133.99 (3) Å) and tetragonal lattice parameters (a = 3.666 (7) Å, c = 5.094 (9) Å and V = 68.47 (9) $Å^3$ were found in good agreement with the (JCPDS CAS No. 27-0997 and 17-0923, respectively) literature [6,12]. Therefore, presence of monoclinic phase is ruled out but due to too many similarities between cubic and tetragonal phase, it is difficult to assign the correct crystal system [6,12,13,18].

In order to resolve the issue Rietveld profile refinement of XRD was first conducted in the highest symmetrical fcc phase of ZrO_2 in the fcc space group F m -3 m (No. 225, Z=1). Best fitted XRD pattern in fcc symmetry is presented in Fig 2(a) and the refined structural parameters are presented in table 1. Further, the XRD pattern was also refined in the tetragonal space group: P 42/nmc. Excellent profile fitted XRD pattern in tetragonal symmetry is illustrated in Fig. 2 (b) and the refined values of crystallographical parameters are presented in table 1. The refined crystallographical parameters for the two phases are found to be in close agreement with literature and the agreement factors listed in table 1 affirmed good profile fittings and thus, validates the refined parameters. Notably it is clearly evident that the profile fitting and agreement factors corresponding to tetragonal phase are superior to cubic system. Thus, it is concluded that our ZrO_2 NPs are crystallized in the phase pure tetragonal symmetry. Correctly assigned Miller indices are marked on the XRD pattern observed/allowed in Fig.1 and the list of reflections are presented in table 1, which are in excellent agreement with literature. In summary, our findings affirmed phase purity and good crystallinity of ZrO_2 NPs in the tetragonal symmetry. Figure 3 shows the 3 D atomic diagram of tetragonal unit cell of ZrO_2 NPs, obtained from the Rietveld refinement using the Vista program.

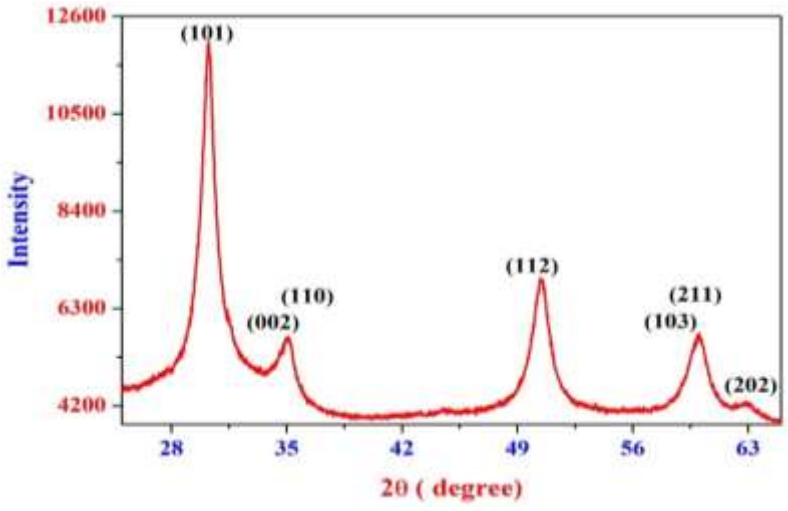

Fig. 1: PXRD pattern of greenly synthesized ZrO_2 NPs.

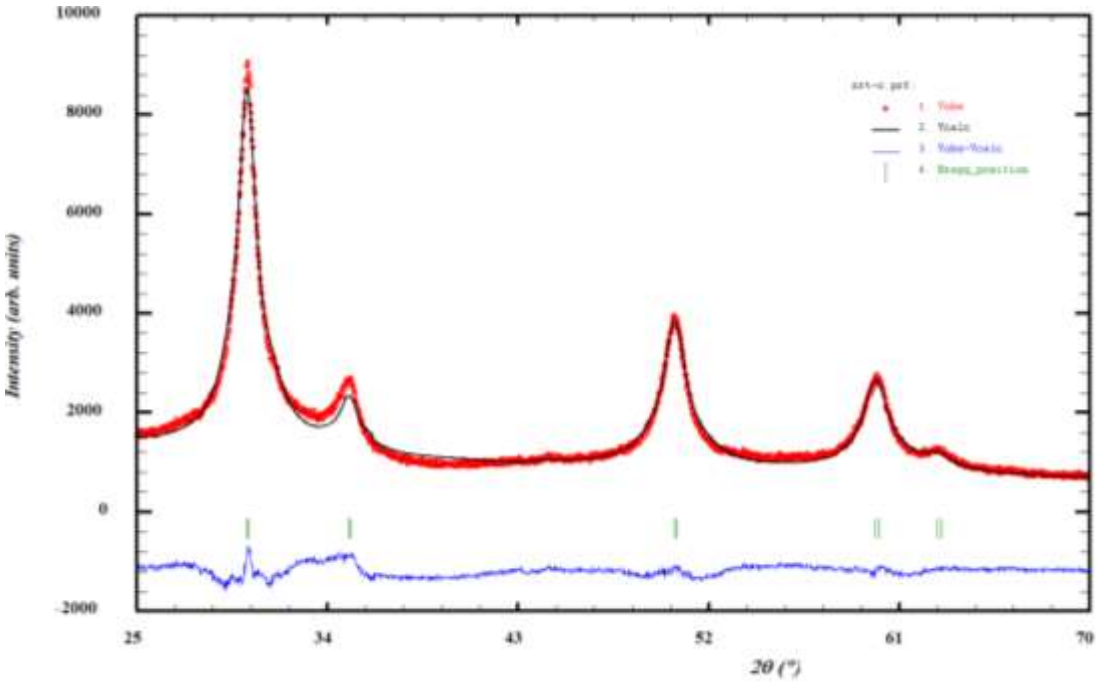

(a)

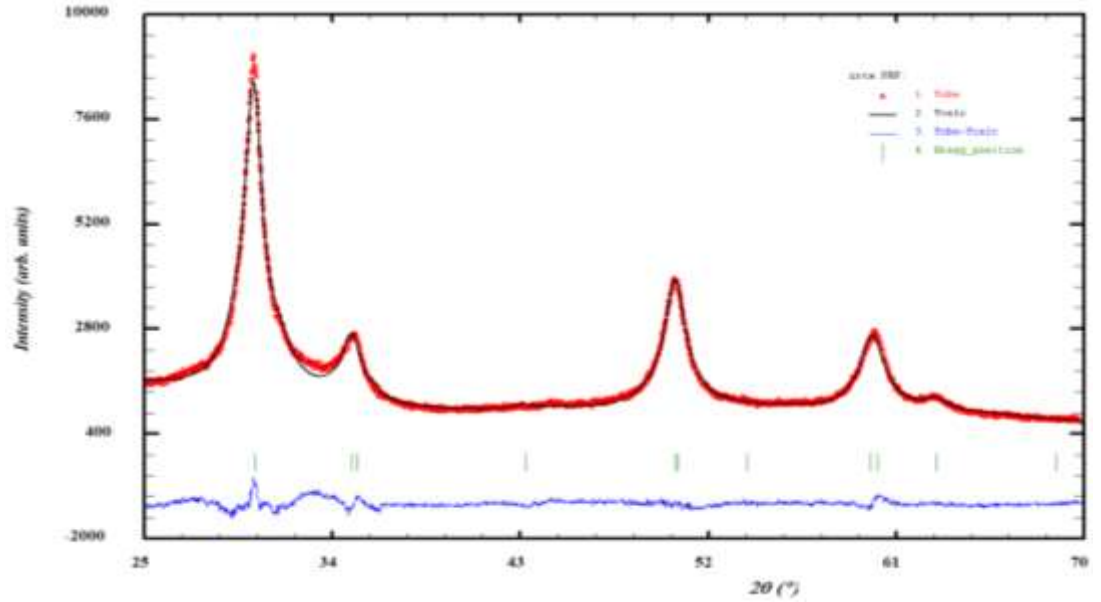

(b)

Fig. 2: Best fitted Rietveld refined XRD pattern of (a) cubic and (b) tetragonal ZrO_2 NPs.

Table 1: Refined **s**tructural parameters and agreement factors of profile refinement of ZrO_2 NPs.

Crystal structure:	**Face centered cubic**
Space group:	F m -3 m (No. 225, Z=1) Zr ions (4a site) at (0.0, 0.0, 0.0) and Oxygen ions (8c site) at (0.25,0.25, 0.25)
Lattice parameters: Reliability factors:	a = 5.120 (1) Å V = 134.24 (2) $Å^3$ Density ρ= 5.11 g/cc R_p = 4.88, R_{wp} = 6.18, R_{exp} = 2.69, R_{Bragg} = 4.08, R_f =3.83, χ^2 = 5.28

Crystal structure:	**Tetragonal**
Space group:	P 42/nmc (No. 137, Z=2) Zr ions (2b site) at (0.75, 0.25, 0.25) and Oxygen ions (4d site) at (0.25,0.25, 0.46 (2))
Lattice parameters: Reliability factors:	a = 3.607 (2) Å c = 5.132 (2) Å V = 66.76 (4) $Å^3$ Density ρ= 6.14 g/cc R_p = 3.45, R_{wp} = 4.42, R_{exp} = 2.48, R_{Bragg} = 1.31, R_f =1.82, χ^2 = 3.17

List of observed/allowed Bragg peaks in tetragonal ZrO_2 NPs

S.No.	(H K L)	FWHM (degree)	2θ (degree)	d_{hkl} (Å)	I_{cal}	I_{obs}
1	(101)	1.20	30.26	2.95	100	100
2	(002), (110)	1.26 1.25	34.94 35.16	2.56	20	19
3	(112)	1.32	50.45	1.807	43	42
4	(103), (211)	1.40 1.41	59.79 60.01	1.545	33	32
5	(202)	1.44	62.94	1.48	5	5

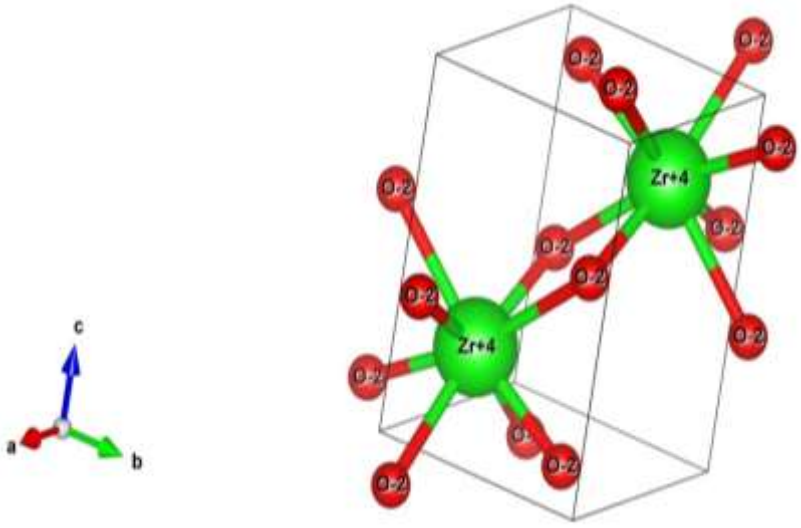

Fig. 3: Tetragonal unit cell of ZrO_2 NPs.

Moreover, massive broadening in the Bragg reflections is directly indicative for the nanocrystalline nature of ZrO_2 NPs. In order to correctly estimate the size of ZrO_2 crystallites band lattice strain in tetragonal lattice of ZrO_2 NPs, following methods were utilized [20]. The peak positions and corresponding full width at half maxima (FWHM) of various planes (listed in table 1) were used for the crystallite size and lattice strain estimation [19,21].

3.2 Crystallite size and lattice strain estimation

3.2.1 Scherrer formula (SF)

The Scherrer formula given below is most common and simplest route for estimating mean size of nanocrystallites.

$$D = \frac{k\lambda}{\beta \cos\theta}; \quad (1)$$

Here, D is the mean crystallite size, λ is x-ray wave length (λ= 0.15405 nm for CuKα), β is FWHM in radians, k = 0.9 is related to the crystallite shape and θ is the diffraction angle of Bragg peak in radian. The FWHM of well resolved and most intense (101) was taken into account and the deduced mean size of ZrO_2 NPs is estimated to 6.7 nm.

3.2.2 Scherrer equation average function (SEAF)

In this method, FWHM of all peaks (see table 1) were utilized in the calculation crystallite size. The calculated size values of crystallite size were averaged. The value of crystal size for each plane and their average mean value are presented in table 2. The mean size of nano crystallites is found to be 6.2 nm, which is slightly smaller than that estimated by Scherrer formula.

Table 2: Crystallite size obtained using SEAF technique for ZrO_2 NPs.

S.No.	HKL	FWHM (β) (radians)	Crystallite size $\frac{k\lambda}{\beta cos\theta}$ (±1) nm	Average crystallite size (±1) nm
1	(101)	0.021315881	6.7	6.2
2	(002), (110)	0.021966766	6.6	
3	(112)	0.024796591	6.2	
4	(103), (211)	0.02714686	5.9	
5	(202)	0.027998903	5.8	

3.2.3 Linear straight-line fit (LSLF)

In this method, the Scherrer equation rearranged as linear straight-line function as:

$$cos\theta = \frac{k\lambda}{D}.\frac{1}{\beta} \quad (2)$$

The plot between cos θ (on y-axis) and $\frac{1}{\beta}$ (on x-axis) shown in Fig. 4 is fitted with eq^n (2). The obtained slope is found to be 0.1003 and the mean size of crystallites size obtained as 13.8 nm. This value of mean size is quite higher than the value computed using other two techniques discussed in previous section.

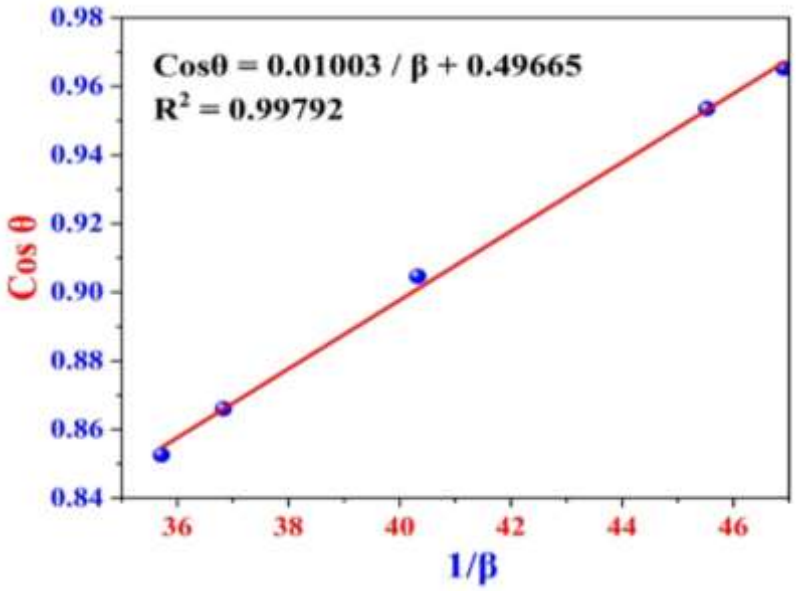

Fig. 4: Best linear straight line fitted graph for ZrO_2 NPs

3.2.4 Straight line passing through the origin technique (SLPOT)

In this technique a line passing through the origin with a slope given below:

$$\text{Slope} = \frac{x_1y_1 + x_2y_2 + x_3y_3 + \ldots\ldots\ldots\ldots\ldots + x_ny_n}{x_1^2 + x_2^2 + x_3^2 + \ldots\ldots\ldots\ldots + x_n^2} \quad (3)$$

The values of x_1, y_1 are extracted and summarized in table 3. The slope equal to $\frac{k\lambda}{D}$ is found 0.01719 and the crystallite size is estimated as 6.3 nm.

Table 3: The (x, y) values extracted from Fig. 2 for ZrO_2 NPs.

x	35.7	36.84	40.29	45.52	46.89
y	0.85	0.87	0.9	0.95	0.97

3.2.5 Monshi-Scherrer formula (MSF)

Monshi-Scherrer formula is also called as modified Scherrer technique. The MSF equation is given below.

$$\beta = \frac{k\lambda}{D} \times \frac{1}{cos\theta} \quad (4)$$

and

$$\ln\beta = \ln\frac{k\lambda}{D} + \ln\frac{1}{cos\theta} \quad (5)$$

A plot between $\ln\beta$ (on y-axis) and $\ln\frac{1}{cos\theta}$ (on x-axis) fitted with a linear equation ($y = mx + c$) give rise to

$$\ln\frac{k\lambda}{D} = \text{Intercept} \quad (6)$$

$$\& \ \frac{k\lambda}{D} = e^{(intercept)} \quad (7)$$

Fig. 5 depicts a slope of 2.19994 and R^2 is 0.99915 along with a negative intercept equal to 3.92316. The obtained value of average crystallite size is 7nm.

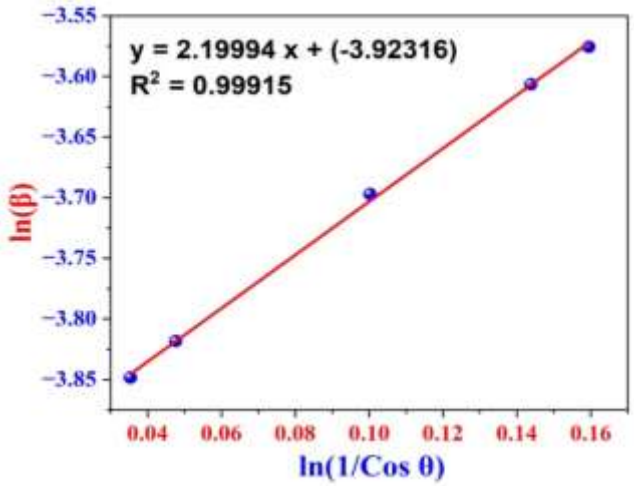

Fig. 5: Linear fit to MSF for ZrO_2 NPs.

Further, in order to taken account the lattice strain, the following three methods were utilized.

3.2.6 Williamson-Hall plot (WHP)

In this technique, the FWHM is as considered combination of both size and strain.

$$\beta = \text{FWHM}_{\text{total}} = \text{FWHM}_{\text{size}} + \text{FWHM}_{\text{strain}} \quad (8)$$

Since the crystal imperfection will give rise to Lattice strain as.

$$\varepsilon = \frac{\beta_{strain}}{4\ tan\theta} \quad (9)$$

So that

$$FWHM_{total} = \frac{k\lambda}{\beta\ cos\theta} + \frac{\beta_{strain}}{4\ tan\theta} \quad (10)$$

The eq^{n} is rearranged as

$$FWHM_{total}.cos\theta = \frac{k\lambda}{D} + 4\varepsilon sin\theta \quad (11)$$

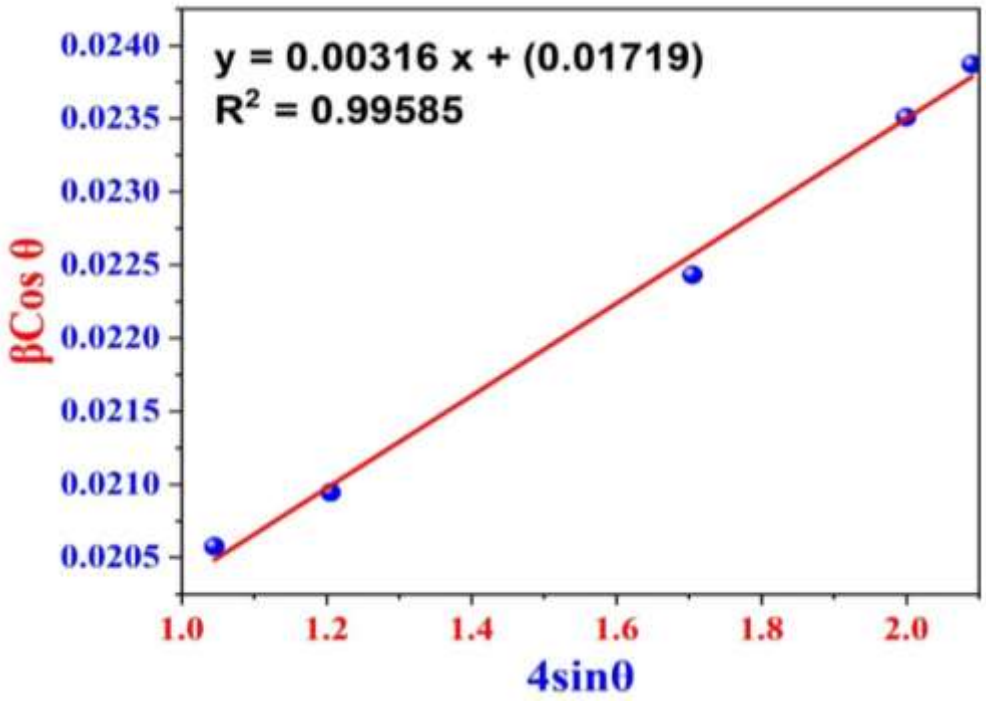

Fig. 6: Best fitted WHP with a linear equation for ZrO_2 NPs.

Fig. 6 demonstrates a plot between $4sin\theta$ (on the x-axis) and $\beta cos\theta$ (on the y-axis). Best linear fitting provided intercept = 0.01719 and slope = 0.00316. The intercept = $\frac{k\lambda}{D}$ and slope provided 8 nm mean size of NPs and a positive strain (tensile strain) = 3.16×10^{-3}.

3.2.7 Size-strain plot formula (SSPF)

In this method, a Lorentz function is considered for size broadening and a Gaussian function corresponding to strain broadening are taken account.

$$\beta_{hkl} = \beta_L + \beta_G \quad (12)$$

Here, β_L and β_G are the FWHM of fitted Lorentz and Gaussian functions, respectively.

The size strain formula is given as:

$$(d\beta cos\theta)^2 = \frac{k\lambda}{D} \times (d^2\beta cos\theta) + \frac{\varepsilon^2}{4} \quad (13)$$

Here, d is the interplanar spacing. In Fig. 7 a plot between $(d\beta cos\theta)^2$ (on y-axis) and $(d^2\beta cos\theta)$ (on x-axis), provided slope $=\frac{k\lambda}{D} = 0.01915$. The deduced crystallite size is 7.2 nm and, lattice strain = 31.7×10^{-3}.

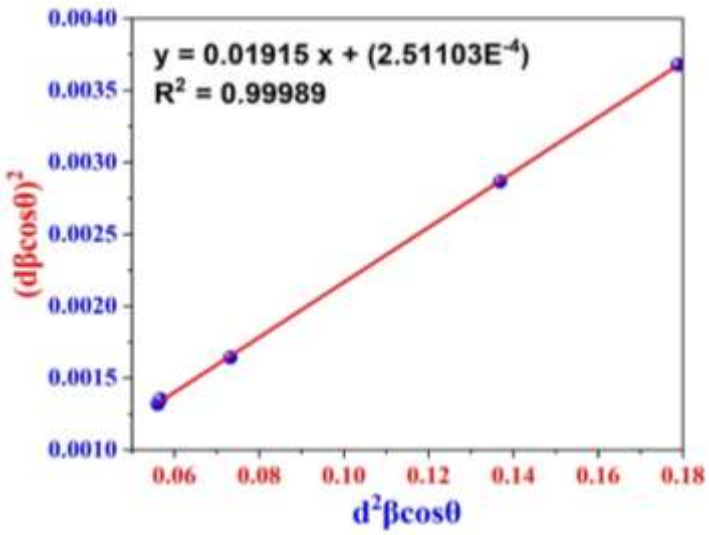

Fig. 7: Linear fit to SSPF for ZrO_2 NPs.

3.2.8 Halder-Wagner formula (HWF)

In this method the size broadening of the peaks are considered as symmetric Voigt function and the HWF formula is given as.

$$\beta_{hkl}^2 = \beta_L \times \beta_{hkl} + \beta_G^2 \quad (14)$$

Here, β_L and β_G are FWHM of Lorentz and Gaussian profile, respectively.

The computational formula of HWF is described as.

$$\left(\frac{\beta^*}{d^*}\right)^2 = \frac{K\beta^*}{D(d^*)^2} + (2\varepsilon)^2 \quad (15)$$

$$\beta^* = \frac{\beta cos\theta}{\lambda} \quad (16)$$

$$d^* = \frac{2dsin\theta}{\lambda} \quad (17)$$

So that $\left(\frac{\beta}{tan\theta}\right)^2 = \frac{k\lambda}{D}\frac{\beta cos\theta}{sin^2\theta} + 16\varepsilon^2$ (18)

Fig. 8 depicts a plot between $\frac{\beta cos\theta}{sin^2\theta}$ (on x-axis) and $\left(\frac{\beta}{tan\theta}\right)^2$ (on y-axis) with a slope = $\frac{k\lambda}{D}$ = 0.01923. The calculated crystallite size is estimated to 7.2 nm and lattice strain = 5.0×10^{-3}.

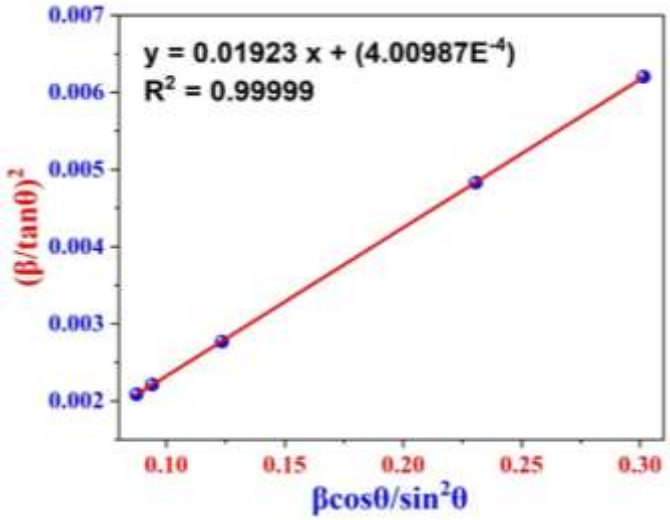

Fig. 8: Linear fit to plot of HWF for ZrO_2 NPs.

Table 4: Deduced mean size value of nanocrystallites and dislocation density of ZrO_2 NPs.

S.No.	Method	Mean nano-crystallite size (D) (±1) nm	Dislocation density $\left(\frac{1}{D^2}\right) \times 10^{-3}$	Lattice strain
1.	SF	6.7	22.2	-
2.	SEAF	6.2	26	-
3.	LSLF	13.8	5.25	-
4.	SLPOF	6.3	25.2	-
5.	MSF	7	20.4	-
6.	WHF	8	15.6	3.16×10^{-3}
7.	SSPF	7.2	19.3	31.7×10^{-3}
8.	HWF	7.2	19.3	5.0×10^{-3}

The deduced value of mean crystallites size and lattice strain obtained using eight methods are presented in table 4. It is clearly evident that except LSLF, all other techniques provided nearly equal values of crystallite size. Although strain parameter obtained in three techniques differs significantly with each other. Similar trend is observed for the dislocation density of ZrO_2 NPs.

3.3 HRTEM analysis

Finally, in order to visibly judge the nanocrystallinity in ZrO_2 NPs, the HRTEM images are recorded. Fig. 8 illustrates the nano metric size particles of ZrO_2 NPs. Size of nearly hundred particles were calculated using the ImageJ software and plotted them in the form of size histogram. The size histogram was fitted with Gaussian profile (Fig. 9(c), Lorentzian profile (Fig. 9(d)) and lognormal profile (Fig. 9(e)). The mean size of nanoparticles obtained by Best fitted profiles is listed in table 5. Interestingly, all three provided nearly same mean size of ZrO_2 NPs. The mean size obtained using lognormal profile and WHP method on account of the lattice strain is appears to be best. The mean nanoparticle size in table 5 & mean crystallite size in table 4 are in good agreement with each other.

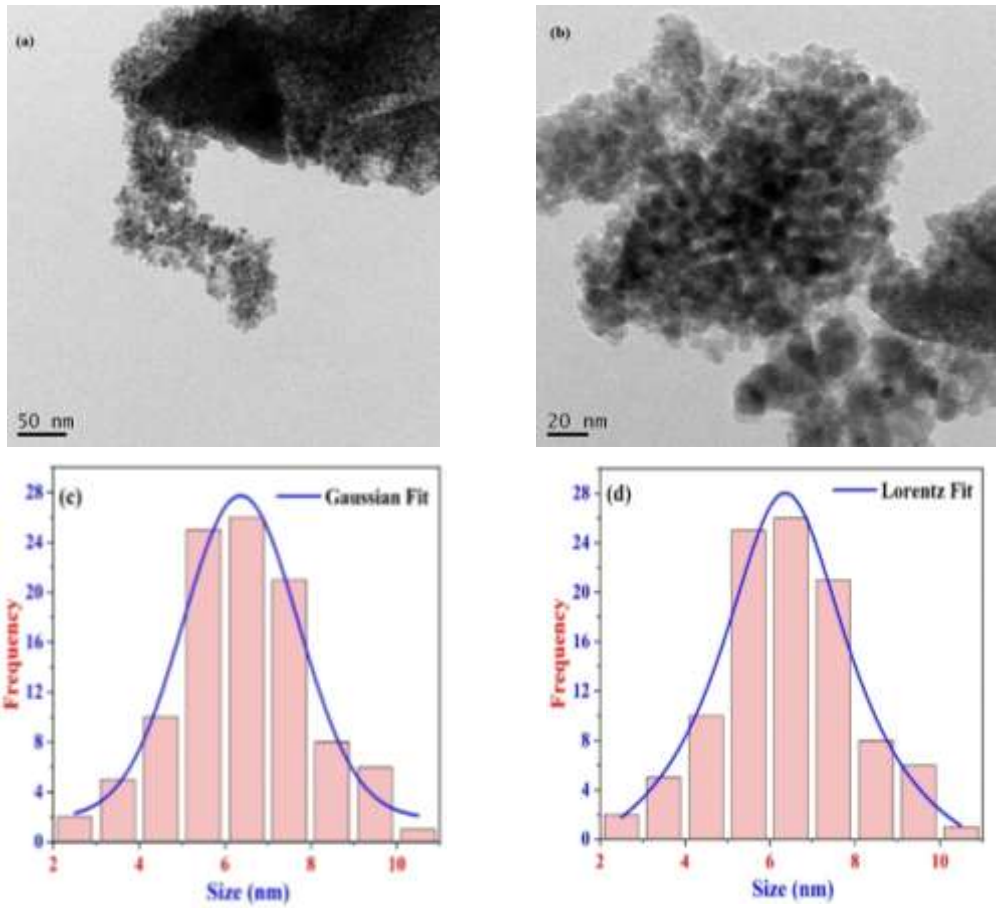

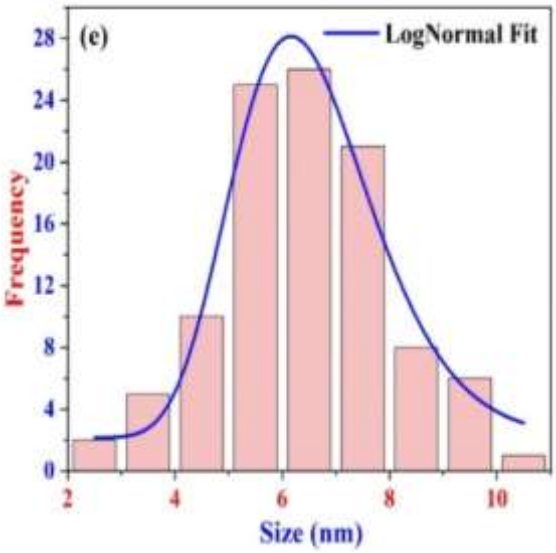

Fig. 9: (a, b) HRTEM micrographs and Size plot histograms fitted with (c) Gaussian, (d) Lorentzian and (e) lognormal functions for ZrO_2 NPs.

Table 5: Deduced mean size values for the nanoparticles of ZrO_2 NPs.

S.No.	Fitting profile Function	Nano particle size (± 2) nm
1.	Gaussian	6.36
2.	Lorentzian	6.36
3.	Lognormal	6.43

4. Conclusions

Micro-structural parameters of ZrO_2 QDs were refined using various strategies. Powder-X and Rietveld refinement of XRD data affirmed phase pure tetragonal structure of ZrO_2 NPs. Mean size of crystallite equal to 8nm, lattice strain = 3.16×10^{-3} and average particle size equal to 6.43 nm are deduced using Williamson-Hall method & lognormal fit to HRTEM. For precise determination of crystal structure Rietveld refinement is must and W-H method is simple and best technique for size and strain analysis, which must be compared with HRTEM data for precise size determination.

Acknowledgements: The authors are thankful to the Referee for valuable comments and suggestions. Vinod Kumar is thankful to CSIR for the NET-JRF fellowship. The authors acknowledge DST-FIST and UGC-MRP for chemicals and material synthesis facility; Jiwaji University for XRD, SAIF-IIT Bombay for the HRTEM facilities.

References

[1] Ahmed, M. F., Podder, M., Moni, M. R., Rahman, M. L., Biswas, B., Khanam, J., Hakim, M., Rahman, M., Hossain, M. S., and Sharmin, N. (2025). Investigation the effect of calcination heating rate on the structural, morphological, thermal and color properties of nano Cobalt Aluminate ($CoAl_2O_4$). Heliyon **11**, e42413.

[2] Bhoi, H., Tiwari, S., Lal, G., Jani, K. K., Modi, S. K., Seal, P., Saharan, V., Modi, K. B., Borah, J. P., Punia, K., Kumar, S. (2022). Green synthesis and characterization of $Mg_{0.93}Na_{0.07}O$ nanoparticles for antimicrobial activity, cytotoxicity and magnetic hyperthermia, Ceram. Int. **48**, 28355-28373.

[3] Bhoi, H., Tiwari, S., Manisha, Hirdesh, Pascual, L., Kumar, S. (2024). Structural, optical, luminescent and magnetic properties of Gd_2O_3 nanoparticles: A comparative study on the effect of different green fuels in the sol–gel synthesis tactics, Inorg. Chem.Commun. **170**, 113487.

[4] Chitoria, A. K., Mir, A., Shah, M. A. (2023). A review of ZrO_2 nanoparticles applications and recent advancements, Ceram. Int. **49**, 32343-32358.

[5] Dong, C. (1999). PowderX: Windows-95-based program for powder X-ray diffraction data processing, J. Appl. Cryst. **32**, 838.

[6] Jayakumar, S., Ananthapadmanabhan, P. V., Thiyagarajan, T. K., Perumal, K., Mishra, S. C., Suresh, G., Su, L. T. and Tok, A. I. Y. (2013). Nanosize stabilization of cubic and tetragonal phases in reactive plasma synthesized zirconia powders, Mater. Chem. Phys. **140**, 176-182.

[7] Joshi, P., Tiwari, S., Punia, K. and Kumar, S. (2022). Defect mediated mechanism in greenly synthesized undoped, Al^{+3}, Cu^{+2} and Zn^{+2} doped TiO_2 nanoparticles for tailoring bandgap, luminescence, magnetic and electrical properties, Opt. Mater. **132**, 112778.

[8] Joshi, P., Tiwari, S. and Kumar, S. (2025). A comprehensive study on the impact of Al doping on the micro-structural, optical and magnetic characteristics of greenly synthesized $Al_xTi1_{-x}O_2$ (x = 0.03–0.15) UFNPs, Mater. Sci. Eng. B **313**, 117997.

[9] Joshi, P., Tiwari, S. and Kumar, S. (2025). A comprehensive study on the impact of La doping on the microstructural, optical, luminescence and magnetic characteristics of greenly synthesized $La_xTi1_{-x}O_2$ QDs, App. Phys. **A 131**, 88.

[10] Khan, S. A., Fu, Z., Rehman, S. S., Asif, M., Wang, W. and Wang, H. (2014). Study of template-free synthesis hierarchical m-ZrO_2 nanorods by hydrothermal method, Powder Tech. **256**, 71-74.

[11] Mobarak, M. B., Hossain, M. S., Chowdhury, F., Ahmed, S. (2022). Synthesis and characterization of CuO nanoparticles utilizing waste fish scale and exploitation of XRD peak profile analysis for approximating the structural parameters, Arabian Journal of Chemistry **15**, 104117.

[12] Ni, S. and Li, Y. (2018). t ZrO_2 prepared by a novel zirconium oxalate synthesised solvothermally, Micro Nano Lett. **13**, 919-922.

[13] Ponkumar, S., Prakashbabu, D., Parasuraman, K., Uthrakumar, R. and Kaviyarasu, K. (2024). Synthesis, characterization, and enhanced photoluminescence of ZrO_2: Dy^{3+} phosphors by incorporating Li^+, Na^+ and K^+ ions for LED applications, Ceram. Int. **50**, 13219-13228.

[14] Prakashbabu, D., Krishna, R. H., Nagabhushana, B. M., Nagabhushana, H., Shivakumara, C., Chakradar, R. P. S., Ramalingam, H. B., Sharma, S. C. and Chandramohan, R. (2014). Low temperature synthesis of pure cubic ZrO_2 nanopowder: Structural and luminescence studies, Spectrochim. Acta A Mol. Biomol. Spectrosc. **122**, 216-222.

[15] Rodriguez-Carvajal, J. (1993). PROGRAM FullProf.2k (Version 8.20 - Feb2025-ILL JRC), Physica B. **192**, 55.

[16] Thakur, M., Vij, A., Kumar, A., Koo, B. H., Singh, F., Rangra, V. S. (2023). Electronic structure and defect induced luminescence study of phase stabilized t ZrO_2 nanocrystals, Luminescence **38**, 762-771.

[17] Thakur, M., Vij, A., Kumar, A., Koo, B. H., Singh, F., Rangra, V. S. (2024). Structural and optical studies of annealed zirconia nanocrystals: Phase transformations, defect dynamics, and magnetic behaviour, Ceram. Int. **50**. 50680-50689.

[18] Tiwari, S., Bano, A., Kamali, S., Williams, A., Johnson, J., Johnson, C., Anandhi, J. S., Patil, S. A., Khot, V. M. and Roychowdhury, P., A. Eyal and S. Kumar (2025). Comprehensive scrutiny on the low temperature magnetism and hyperthermia efficiency of greenly synthesized biocompatible $Zn_{0.25}Ca_{0.25}Fe_{2.5}O_4$ nanoparticles, J. Phys. D: Appl. Phys. **58**, 105001.

[19] Xing, Z., Pang, Y., Li, E., Zhang, J. Y., Xu, D. (2024). Preparation and characterisation of zirconia/hydroxyapatite bioactive composites as potential dental implants, J. Mater. Sci.: Mater. Eng. **19**, 1-13.

[20] Zhang, W., Zhang, H., Abbas, M., Zhang, J., Huang, Z., Kawi, S. and Chen, J. (2024). Ecofriendly solid-state synthesis of Na-promoted Mn-Fe/ZrO_2 catalyst for Fischer-Tropsch synthesis, Fuel **363**, 131013.

[21] Zhang, Y., Chen, H. X., Duan, L., Fan, J. B., Ni, L. and Ji, V. (2018). A comparison study of the structural and mechanical properties of cubic, tetragonal, monoclinic, and three orthorhombic phases of ZrO_2, J. Alloys Compd. **749**, 283-292.